IEEE Access
Multidisciplinary | Rapid Review | Open Access Journal

Received February 9, 2021, accepted March 1, 2021, date of publication March 10, 2021, date of current version March 26, 2021.

Digital Object Identifier 10.1109/ACCESS.2021.3065576

Central Blood Pressure Estimation From Distal PPG Measurement Using Semiclassical Signal Analysis Features

PEIHAO LI AND TAOUS-MERIEM LALEG-KIRATI, (Senior Member, IEEE)

Computer, Electrical and Mathematical Sciences and Engineering Division, King Abdullah University of Science and Technology (KAUST), Thuwal 23955, Saudi Arabia

Corresponding author: Taous-Meriem Laleg-Kirati (taousmeriem.laleg@kaust.edu.sa)

This work of Taous-Meriem Laleg-Kirati was supported by the King Abdullah University of Science and Technology (KAUST) Base Research under Grant BAS/1/1627-01-01.

ABSTRACT Background and objective: Blood pressure (BP) is one of the crucial indicators that contains valuable medical information about cardiovascular activities. Developing photoplethysmography (PPG)-based cuffless BP estimation algorithms with enough robustness and accuracy is clinically useful in practice, due to its simplicity and noninvasiveness. In this paper, we have developed and tested two frameworks for arterial blood pressure (ABP) estimation at the central arteries using photoplethysmography and electrocardiogram. Methods: Supervised learning, as adapted by most studies regarding this topic, is introduced by comparing three machine learning algorithms. Features are extracted using semi-classical signal analysis (SCSA) tools. To further increase the accuracy of estimation, another BP estimation algorithm is presented. A single feed-forward neural network (FFNN) is utilized for BP regression with PPG features, which are extracted by SCSA and later used by FFNN as the network input. Both BP estimation algorithms perform robustly against MIMIC II database to guarantee statistical reliability. Results: We evaluated the performance against the Advancement of Medical Instrumentation (AAMI) and British Hypertension Society (BHS) standards, and we have compared the standard deviation (STD) of estimation error with current state of the arts. With the AAMI standard, the first method yields comparable performance against existing literature in the estimation of BP values. Regarding the BHS protocol, the second method achieves grade A in the estimation of BP values. Conclusion: We conclude that by using the PPG signal in combination with informative features from the Schrödinger's spectrum, the BP can be non-invasively estimated in a reliable and accurate way. Furthermore, the proposed frameworks could potentially enable applications of cuffless estimation of the BP and development of mobile healthcare device.

INDEX TERMS Blood Pressure (BP), cuffless BP estimation, photoplethysmography (PPG), inappropriate PPG, Schrödinger spectrum, SCSA feature extraction.

I. INTRODUCTION

Blood pressure (BP) is what drives the flow of blood through the blood vessels, thus playing an important role in the dynamics of blood flow in each heartbeat interval. Abnormal blood pressure is currently being considered as a crucial risk factor for cardiovascular diseases [1]. Hypertension, as one of the major aspects leading to the evolution of cardiovascular diseases (CVDs) [2] silently harms internal body organs such as brains, eyes and kidneys, which can also cause strokes, heart attacks, and kidney failure [3]. The negative cardiovascular effects of hypertension have been reported to be largely dependent on absolute BP values and increased blood pressure variability (BPV) [4]. Accurate BP measurement and estimation are vital for prevention, diagnosis, and treatment of hypertension and related CVDs. Depending on the clinical situation, either continuous or intermittent blood pressure monitoring is employed. There are two types of approaches for BP measurement known as invasive and noninvasive measurement. Invasive BP measurement is a highly accurate method available for measuring continuous BP, but it causes potential health issues

The associate editor coordinating the review of this manuscript and approving it for publication was Fan Zhang.

to patients such as bleeding and infection risks, while damages at vascular tissues cause arterial obstruction. Also, in specific clinical situations, there are cases where invasive BP monitoring may be not feasible if safety conditions are not met properly. Korotkoff sounds to estimate SBP and DBP is another accurate and reliable way of BP measurement, but it requires trained professionals and it prevents ambulatory blood pressure measurement (ABPM) [5]. Cuff-based BP measurement equipments are widely used in hospital and home settings to detect abnormal BP [6], however, defects of its discontinuous nature and the discomfort caused by the repeated cuff inflations prevent continuous BP monitoring.

Since most methods for measuring BP waveforms are not convenient for continuous measurement and ABPM applications, recently, there has been an increasing amount of attention in cuffless BP estimation algorithms to enable continuous BP monitoring in an easy way, by mapping features of signals that are easy to measure, to individual's beat to beat BPs. In terms of method simplicity, [7] and [8] have attempted to develop algorithms for cuffless ABP estimation, although their studies have achieved acceptable accuracy using MLR algorithms, their method are subjected to the practical issues of placing two sensors, with will cause movement inconvenience for the users. In fact, most researchers use more than two sensors in their research of cuff-less ABP estimation, [9] has reached fairly well accuracy but also requires two sensors. There are works that utilize only one signal, such as [10], however, multiple magnetic sensors need to be placed in order to obtain pulse wave velocity (PWV) signal, hindering their simplicity to use.

To address these issues, photoplethysmography (PPG) technology has gained considerable interest by being widely applied to wearable sensors [11], the non-invasive estimation of blood pressure (BP) using the PPG method has become a hot topic nowadays. The PPG signal can be separated into systolic and diastolic parts. The systolic part of the signal is related to the process of contraction of the heart while the diastolic part of the signal is related to the process of cardiac expansion. One of the challenges is that, in the intersection of the two parts, there is a split between the systolic and diastolic parts called dicrotic notch. In the recorded samples of some individuals (typically in a patient), the dicrotic notch is not detectable, thus casting doubt on studies where inappropriate PPG signals might result in high errors with unkown effects. [12] develops new methods for estimating BP regardless of the form and shape (appropriate and inappropriate) of PPG signal, but their result falls into grade C in SBP estimation, with BHS standard [13]. Another challenge is that, in studies such as [9], [12], the result slightly exceeds the error boundary of the systolic blood pressure (SBP) requirement [14]. Also, after implementing [3] in the MIMIC II database, we found the algorithm's accuracy slightly decreases. Therefore, increasing the SBP estimation accuracy of existing methods can be of interest. In the following sections, we develop our methods bearing these objectives in mind.

A semi-classical signal analysis (SCSA) method has been proposed for pulse shaped signal analysis in [15]. Application of SCSA to BP waveform has been shown in previous studies [16]. This method has been inspired from a soliton's based method [17]–[19]. The potential is given by the solution of a KdV equation, where each negative eigenvalue is correlated one soliton [17] (Soliton is the solution of some nonlinear partial differential equations like the Korteweg-de Vries (KdV) equation proposed in Crépeau and co-workers [20], [21]). These eigenvalues describe solitons in terms of soliton velocities with the largest eigenvalues describing fast solitons [17]. Therefore, they have been utilized as features in ABP signal. Morover, it has been shown that there is a similarity between the PPG and ABP morphologies, suggesting PPG holds informative features that exist in ABP. [22]. Inspired by previous works, the study proposes two frameworks for beat-to-beat BP estimation based on extracted PPG features. While BP regression analysis has been extensively studied in different research [2], [3], [7]–[9], [11], [23], correlation between PPG signal and BP has been shown. However, when PPG shapes are inappropriate, as is the case with most patients from intensive care units (ICU) affected by drugs, several important features can be difficult to localize and extract. In the first BP estimation framework, a new algorithm for estimating the Diastolic Blood Pressure (DBP), Mean Arterial Pressure (MAP) and Systolic Blood Pressure (SBP) is proposed using the PPG signal with both appropriate and inappropriate shapes. We explains how the SCSA method can decompose systolic and diastolic phase regardness of its appropriateness. PPG waveform segments are decomposed by SCSA and used as features for supervised machine learning. To further increase the accuracy of the SBP estimation, [24] suggests that artificial neural networks (ANNs) have better performance compared to traditional regression analysis techniques using pulse arrival time (PTT). Inspired by this work, we have developed the second framkework using PPG features as ANN input, which solved the SBP estimation boundary issue. The paper is organized as follows. Section II introduces the clinical database we have used throughout this study. Then it outlines the principle of our ABP estimation methodology by describing SCSA method. Moreover, machine learning frameworks used to evaluate ABP are described with experimental results that compare different machine learning algorithms and existing evaluation standards, demonstrating the effectiveness of features extracted from the SCSA method. Section III introduces FFNN's structure and its performance by comparing against the AAMI and BHS standard. The SCSA method is used for feature extraction, and an artificial neural network (ANN) is used for estimation. Section IV presents discussions of our methods and comparison of other methods in more detail. Section V concludes the paper by summarizing our results and contribution.

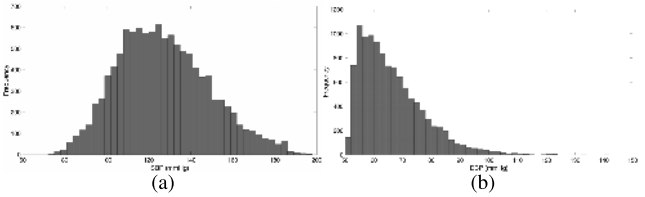

FIGURE 1. Histograms of the database parameters. (a) Systolic blood pressure. (b) Diastolic blood pressur.

TABLE 1. BP ranges in the MIMIC II database.

	Min (mmHg)	Max (mmHg)	STD	Mean
MAP	58.3727	160.9037	12.9134	86.5494
DBP	50.7019	149.0172	11.2655	66.2998
SBP	72.8688	195.7036	21.6798	127.0485

II. PREDICTING BLOOD PRESSURE USING SUPERVISED MACHINE LEARNING ALGORITHMS

A. ONLINE DATABASE AND PREPROCESSING

The Physionet's multiparameter Intelligent monitoring in intensive Care (MIMIC) II online waveform database is used for accuracy analysis and comparison with existing methods. Simultaneous PPG and ABP signals have been recorded for many patients in various intensive care units (ICU), with part of them used in this study.

The ABP signal is used for the extraction of reference BP values, while the PPG signal is used for extraction of SCSA features. Over 8000 instances were used in the database with signals sampled at 125Hz and precision of 8 bits. The ABP signal has been recorded invasively from the aorta and the PPG signal is recorded from the fingertip. In this study, we consider the interval of 40 seconds to estimate BP from the ABP signal. In each signal segment, the minimum and maximum values are considered as DBP and SBP. Accordingly, MAP is calculated by MAP $= (2 \times \text{SBP} + \text{DBP})/3$. The database includes 707567 signal segments which belong to 8000 individual records. In order to remove the adverse influence of noise and artifacts from the raw signals, [25] is followed regarding the preprocessing of the individual records. Fig. 1 and Table 1 demonstrate some statistical information about the distribution and ranges of the DBP, MAP, SBP values in the final processed database.

B. SCSA BACKGROUND

The SCSA method has been recently proposed as an effective tool in analysing pulse shaped signals by Laleg-Kirati *et al.* [15]. Given a real positive signal $y(t)$, SCSA decomposes $y(t)$ into a set of squared eigenfunctions by using the discrete spectrum of the Schrödinger operator. The reconstructed signal $y_h(t)$ is illustrated in eq. 1.

$$y_h(t) = 4h \sum_{n=1}^{N_h} \kappa_{nh} \psi_{nh}^2(t), \quad t \in \mathbb{R}, \tag{1}$$

where $\lambda_{nh} = -\kappa_{nh}^2$ are the negative eigenvalues ($\kappa_{1h} > \kappa_{2h} > \cdots > \kappa_{nh}$), and $\{\psi_{1h}, \psi_{2h}, \cdots, \psi_{nh}\}$ are the corresponding

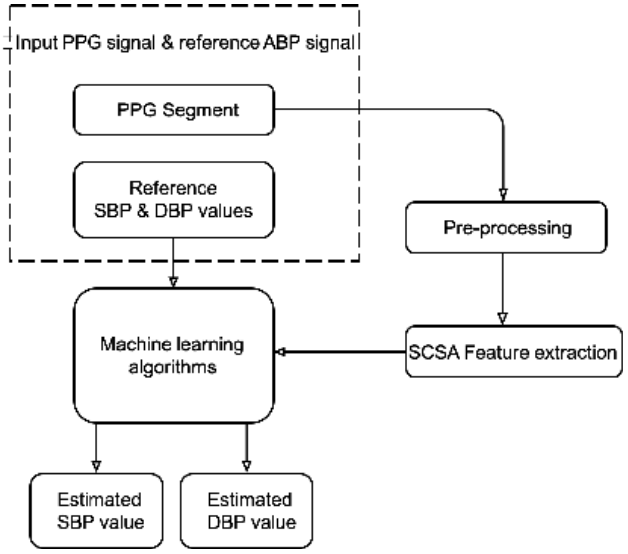

FIGURE 2. The block diagram of ABP estimation methodology.

L_2^2-normalized eigenfunctions ($n = 1, 2, \cdots, N_h$) such that

$$-h^2 \frac{d^2\psi(t)}{dt^2} - y(t)\psi(t) = \lambda\psi(t). \tag{2}$$

N_h is the number of negative eigenfunctions and h is a positive parameter known as the semi-classical constant. N_h is a crucial index when reconstructing the signal. When N_h is relatively large (h tends to zero), the reconstructed spectrum y_h converges to the true spectrum y. This observation is consistent with the semi-classical properties of the Schrödinger operator where N_h increases when h decreases [26], [27]. One of the important characteristics is that eigenfunctions which correspond to large eigenvalues represent the profiles of the peaks, whereas the remaining functions characterize the noise details of these profiles. In the specific case of PPG signal feature extraction, we have tested a range of N_hs and selected N_h for each individual case which properly reconstructs the PPG signal given the similarities in morphology between them.

In Fig. 3, the PPG signal was estimated for several values of the parameter h and thus N_h. In the online dataset, the PPG signal is properly reconstructed when N_h varies in [5, 12] for individual cases.

C. FEATURE EXTRACTION

1) SCSA FEATURES

Each PPG signal waveform can be divided into two parts. The first part of the signal is related to the contraction of the heart orthe systole while the second part is related to cardiac expansion or diastole. Therefore, the application proposes the decomposition of PPG waveform into two partial sums: the first sum is composed of the N_s ($N_s = 1, 2, \cdots, min(3, [N_h/2])$) largest κ_{nh} and the second sum is composed of the remaining κ_{nh} components. The first partial sum describes rapid phenomena of the systolic phase and the second partial sum describes slow phenomena of the

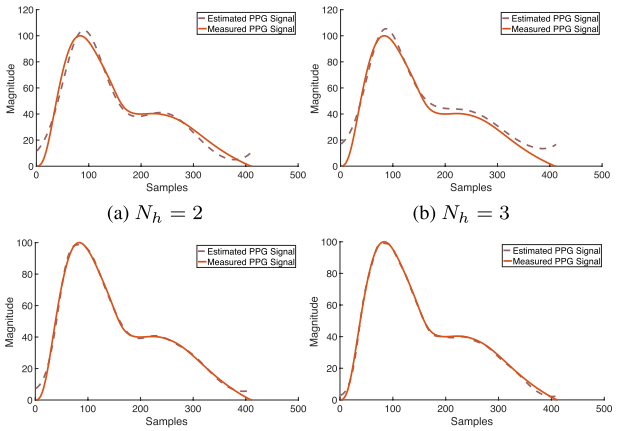

(a) $N_h = 2$ (b) $N_h = 3$ (c) $N_h = 5$ (d) $N_h = 10$

FIGURE 3. Inappropriate PPG shape constructed by SCSA with different N_h values. PPG measured signals (in red) and SCSA decomposed signals (in dotted line). (a)(b) SCSA is recovering the signal shape while ignoring peak details when $N_h = 2$ or $N_h = 3$. (c)(d) With N_h increasing (between [5, 10]), the rest of the signal is also recovered.

diastolic phase. We denote by P_s and P_d the systolic and diastolic dynamics, which are shown in Fig. 4 and Fig. 5, respectively [16].

$$P_s = 4h \sum_{1}^{N_s} \kappa_{nh} \psi_{nh}^2(t) \tag{3}$$

$$P_d = 4h \sum_{N_s+1}^{N_h} \kappa_{nh} \psi_{nh}^2(t) \tag{4}$$

Several different SCSA extracted features are selected from PPG segments in each individual case, which consists of the systolic invariant parameter $\sum_{n=1}^{N_s} \kappa_{nh}$, the diastolic invariant parameter $4h \sum_{N_s+1}^{N_h} \kappa_{nh}$, the whole PPG spectrum parameter $\hat{P}_s + \hat{P}_d$, the PPG spectrum leading parameters κ_{1h}, κ_{2h}. Inspired by [16], the systolic and diastolic invariants are used as the last two features $\sum_{n=1}^{N_s} \kappa_{nh}^3$ and $4h \sum_{N_s+1}^{N_h} \kappa_{nh}^3$. In summary, the SCSA features can be categorized as follows:

- SCSA eigenvalues:

$$\kappa_1, \kappa_2, \cdots, \kappa_{N_h-1}, \kappa_{N_h} \tag{5}$$

- SCSA systolic invariants:

$$\text{INVS}_1 = 4h \sum_{n=1}^{N_s} \kappa_{nh} \tag{6}$$

$$\text{INVS}_2 = \frac{16h}{3} \sum_{n=1}^{N_s} \kappa_{nh}^3 \tag{7}$$

- SCSA diastolic invariants:

$$\text{INVD}_1 = 4h \sum_{N_s+1}^{N_h} \kappa_{nh} \tag{8}$$

$$\text{INVD}_2 = \frac{16h}{3} \sum_{N_s+1}^{N_h} \kappa_{nh}^3 \tag{9}$$

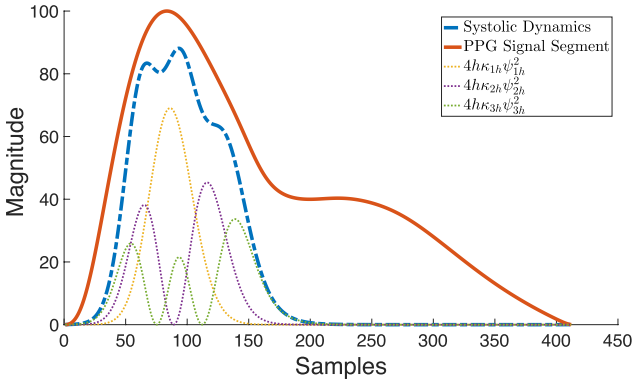

FIGURE 4. Estimated systolic dynamics. PPG measured signals (in red) and SCSA estimated systolic part (in blue dotted line).

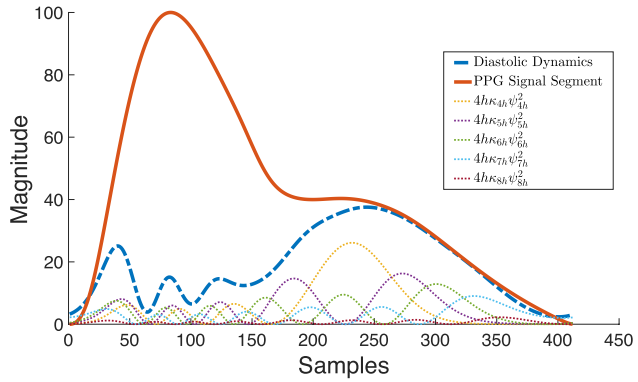

FIGURE 5. Estimated diastolic dynamics. PPG measured signals (in red) and SCSA estimated diastolic part (in blue dotted line).

- SCSA eigenvalue summation:

$$4h \sum_{1}^{N_h} \kappa_{nh} \tag{10}$$

Our approach adapts mainly the SCSA features. One method is using PPG signal waveform only with another method adding ECG signal waveform, called PAT-included features approach. By selecting N_s parameter in a proper way, the PPG signal is separated into two cardiovascular dynamics even when the PPG shape is inappropriate, thus guaranteeing stable and robust feature extraction in the BP estimation process.

2) OTHER FEATURES

Other literature works are mainly using PPG features and ECG features when estimating ABP values, with most of the features extracted from PPG signal waveforms. They are summarized as follows:

a: HEART RATE (HR)

Heart rate is measured by the interval length L between R peaks of ECG signals (Fig. 7). Given the sampling frequency of the ECG signal, HR can be calculated by using

$$\text{HR} = \frac{L}{\text{freq}} \tag{11}$$

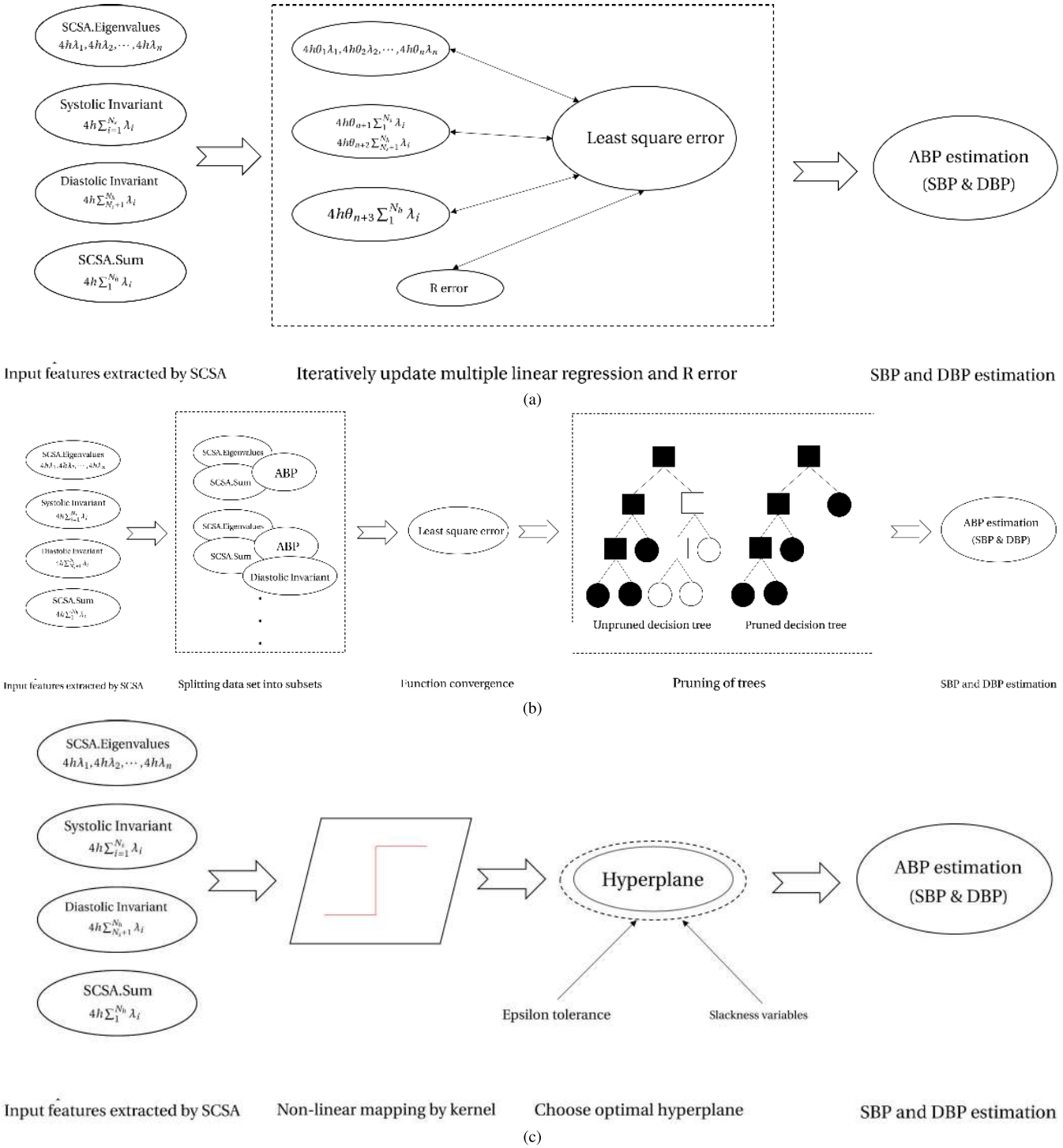

FIGURE 6. (a) Block diagrams of multiple linear regression (MLR). MLR coefficients and the random error are updated in each iteration to converge the least square error function. (b) Block diagrams of the decision tree regression (DTR). Data set is splitted into different subsets and used to converge least square function. Trees are pruned to simplify structure. Each node (small black colour-filled circles) contains an estimation result. (c) Block diagrams of SVM regression. Epsilon and slack variables surrounding the hyperplane contributed to make the dual objective formula with the Lagrangian function to solve the equation for BP estimators.

b: INFLECTION POINT AREA (IPA) RATIO AND WIDTH

Past studies have shown that IPAR is strongly correlated to total peripheral resistance (TPR) [28], which is then selected to extract features for ABP estimation. Inflection Point Area (IPA) Ratio is the ratio of the four pulse areas between selected points in the PPG signal waveform [29], S_1, S_2, S_3 and S_4, which are shown in Fig. 8. Further proposed by [3], the sum of S_ns can be used

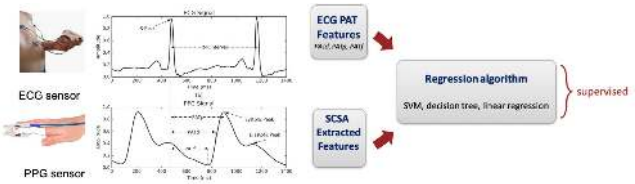

FIGURE 7. A random patient case containing PPG and ECG signal. (Upper)PPG signal. (Lower)ECG signal. The figure demonstrates the calculation of pulse arrival time (PAT) features and heart rate (HR) by locating R peaks as well as the PPG IPAs.

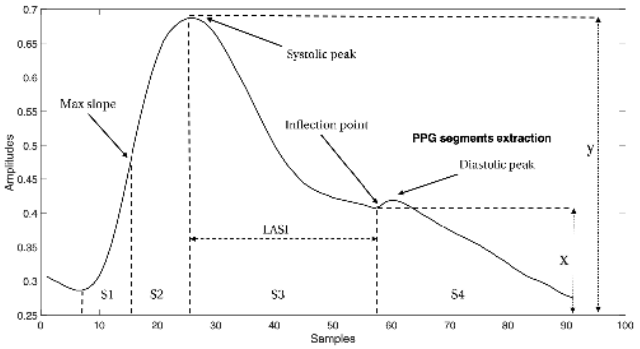

FIGURE 8. PPG waveform features extraction. Inflection point area ratio and width (IPA, labelled S1-S4), large artery stiffness index (labelled LASI) and augmentation index (AI, labelled x and y).

to calculate peak widths and selected as features for estimation.

c: LARGE ARTERY STIFFNESS INDEX (LASI)

Large Artery Stiffness Index (LASI) is an index of the arterial stiffness. LASI is inversely related to the time interval between the inflection point and systolic peak immediately before it (shown in Fig. 8).

d: AUGMENTATION INDEX (AI)

AI is a measure of the wave reflection on the arteries wall [30], which is contributing on systolic arterial pressure. It is calculated by (Fig. 8):

$$\mathrm{AI} = \frac{x}{y} \tag{12}$$

e: PAT FEATURES

Pulse arrival time (PAT) values are widely used by other literature works such as [9] by calculating the distance between the ECG R-peak and IPA characteristic points on the PPG signal (shown in Fig. 7):

- PATp: distance between the ECG R peak and the PPG systolic peak immediately after it.
- PATd: distance between the ECG R peak and the PPG diastolic peak immediately after it.
- PATd: distance between the ECG R peak and the point at which the maximum value of the PPG signal first derivative occurs.

In the PPG signal, there is a splitting point in time scale, which is between systolic and diastolic cardiac phases called dicrotic notch. In MIMIC II database, many recorded samples

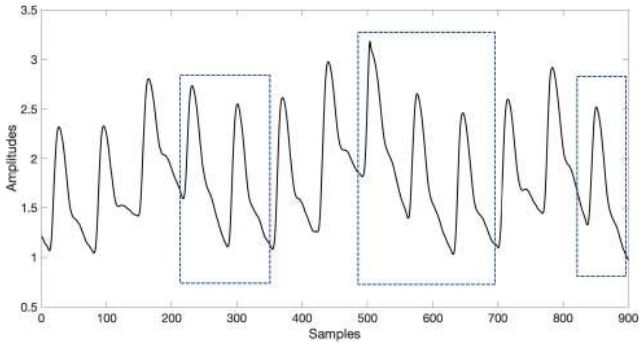

FIGURE 9. Sample PPG waveform from MIMIC II database containing undetectable dicrotic notch (highlighted in dotted frame).

of the PPG signal waveforms from patients affected by drugs or with hypertension, the dicrotic notch is not easy to localize and in some cases it is simply not detectable, shown in Fig. 9

D. MACHINE LEARNING ALGORITHMS

To create the training and testing dataset for supervised machine learning, we divide the periodic ABP signal into separate interval segments to obtain the reference SBP and DBP as target, which corresponds to the maximum and minimum values of the segments. Training features are extracted from simultaneously obtained PPG segments. The proposed methodology can continuously estimating the ABP (SBP and DBP) with the estimation frequency that depends on the subject's heart rate (HR), normally in an order of seconds. The estimation process is considered as continuous in contrast to sensor measurement frequency (in milliseconds) depending on specific sensor types and sampling and measurement frequency settings. While same feature vectors (with each element containing one SCSA extracted feature) are used for the prediction of the SBP, DBP, different machine learning models are trained to estimate targets. The models are illustrated as follows.

1) MULTIPLE LINEAR REGRESSION (MLR)

Multiple linear regression fits a linear equation to observed data, which models the relationship between two or more multiple variables and one target variable. MLR has been widely used by previous researchers for cuffless ABP estimation [7], [23], [31]. This algorithm selects correlation coefficients $\theta_1, \theta, \cdots, \theta_n$. As shown in Fig. 6a, each input features are associated with one θ, which gets iteratively updated with least square algorithm to minimize the regression error (R.error), shown in eq. 13.

$$\begin{aligned} J(\theta_1, \theta_2, \cdots, \theta_{n+2}) &= \frac{1}{m}\sum_{i=1}^{m}(h_\theta(x^{(i)}) - y \\ h_\theta(x) &= 4h\theta_1\lambda_1 + 4h\theta_2\lambda_2 + \cdots + 4h\theta_n\lambda_n \\ &\quad + 4h\theta_{n+1}\sum_{1}^{N_s}\lambda_i + 4h\theta_{n+2}\sum_{N_s+1}^{N_h}\lambda_i \\ &\quad + 4h\theta_{n+3}\sum_{1}^{N_h}\lambda_i + \epsilon. \end{aligned} \tag{13}$$

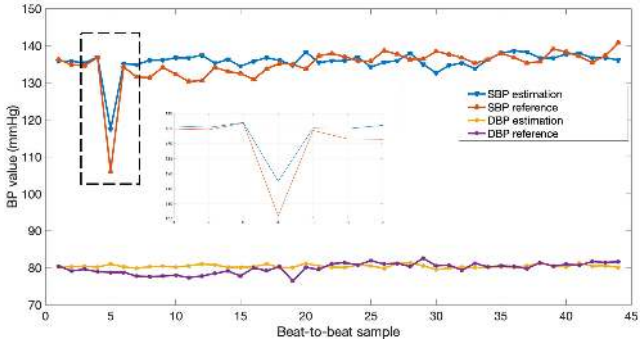

FIGURE 10. Realtime BP estimation. SBP estimation (in blue) catching SBP reference (in red) at sample index around 5 (labelled in long dashed line).

where m is the number of training samples in datasets. ϵ is bias coefficient plus some random error. $\theta_{0-(n+3)}$ are coefficients. λ_{1-N_h} is SCSA eigenvalues, with the number of eigenvalues being N_h.

2) SUPPORT VECTOR MACHINE (SVM)

Support Vector Machine (SVM) can be used as a regression method, maintaining all the main features that characterize the algorithm by using kernel function [3], [9]. SVM regression has a similar working principle as in the least square method of MLR to minimize the error function (squared error between the predicted and reference SBP and DBP), with different approaches of minimizing the error function. SVM tries to maximize the margin between the closest support vectors, which helps pushing the limitations subjected to distributional properties of underlying variables, geometry of the data and the common problem of overfitting.

3) DECISION TREE

Decision Tree algorithm is a faster algorithm in training process compared to SVM algorithm, without the need to normalize and scale data, thus requiring less effort in data preparation. It follows the same approach as humans generally follow while making decisions, which propagates decisions from the root nodes to the leaf nodes in numeric form. It splits the dataset with the best optimization criteria. The process includes splitting input data into subsets and pruning that reduces the size of decision trees by removing branches and leaves of the tree that provide little power to classify instances, shown in fig. 6c.

E. RESULTS

The ABP estimation methodology as stated above is applied to the data selected from MIMIC II database. We have chosen around 8000 individuals for feature extraction and prediction evaluation. We evaluate the algorithm performance by averaging MAE and STD out of records, each each records containing 40 seconds sampling time.

MLR, SVM and regression tree are evaluated in terms of overall ABP estimation accuracy. After training with 70% of the signal segments with the remaining 30% to predict,

TABLE 2. Comparison of the performance using SCSA feature sets in various learning algorithms.

	SBP (mmHg)		DBP (mmHg)	
	MAE	STD	MAE	STD
Support Vector Machine	**7.44**	**7.37**	**5.09**	**5.66**
Multiple Linear Regression	8.94	9.76	5.90	7.11
Decision Tree	8.47	9.29	5.42	6.36

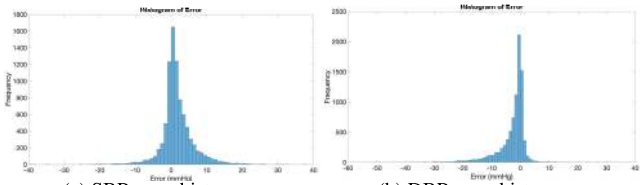

(a) SBP error histogram (b) DBP error histogram

FIGURE 11. SBP and DBP error histogram from the SVM regression.

each case contains reference ABPs (mmHg), estimated ABPs (mmHg), and the error (mmHg) given by the absolute difference between reference and estimated ABPs. The ABPs (including both reference and estimated ABPs) are calculated for each case based on certain segment in that case. In comparison, all the methods show acceptable prediction accuracy by training with the SCSA features

In Table 2, the MAE and STD of estimated ABPs are calculated for the three machine learning algorithms respectively based on estimation cases as an overall ABP estimation evaluation. The result shows that the SVM achieves the smallest mean average error of SBP (7.44 mmHg difference between reference and predicted SBP) while also achieves the smallest STD (7.37 mmHg) when compared with the regression tree and SVM algorithms. Similarly, the decision tree and has shown an acceptable MAE and STD (by not exceeding 10 mmHg). It is also observed that SVM performance is leading in the three algorithms by providing better estimation in terms of SBP and DBP.

Fig. 11a and 11b present the results in histograms of estimation error, when using PPG features only, extracted by SCSA. The histograms show that error values are approximately distributed around zero. It can be seen from Table 2 that the STD of SBP is larger than the STD of DBP, which is the underlying reason explaining why the histograms show greater estimation errors for SBP values comparing with estimation errors for DBP values.

1) ASSOCIATION FOR THE ADVANCEMENT OF MEDICAL INSTRUMENTATION STANDARD (AAMI)

Table 6 demonstrates a comparison between the results of our ABP estimation methodology with the AAMI standard [14]. The AAMI requires BP measurement devices to have ME less than 5 mmHg and STD less than 8 mmHg. According to Table 6, the proposed method has ME values close to zero, which is much lower than the ME maximum standard margin proposed by the standard. Further, regarding the STD criterion, DBP and MAP values are within the 8 mmHg STD

TABLE 3. Results evaluated by the AAMI standard.

		ME (mmHg)	STD (mmHg)	subjects
Our results	MAP	-0.242	7.138	6760
	DBP	-0.664	7.416	6760
	SBP	0.435	10.225	6760
AAMI [14]		≤ 5	≤ 8	≥ 85

TABLE 4. Comparison with the BHS standard.

		Cumulative Error Percentage		
		≤ 5 mmHg	≤ 10 mmHg	≤ 15 mmHg
Our results	SBP	56.98%	77.28%	86.43%
	DBP	73.54%	87.66%	90.20%
	MAP	69.18%	86.41%	92.77%
BHS [13]	grade A	60%	80%	95%
	grade B	50%	75%	90%
	grade C	40%	65%	85%

standard margin, while the STD value of the SBP estimation is slightly exceeding the standard's limit (10.22 mmHg out of 8 mmHg).

It is also necessary to mention that the AAMI standard requires devices to be evaluated on a sample of at least 85 different subjects. However, we have verified the our ABP estimation methodology on a population of 6760 subjects given the huge number of different individual cases in MIMIC II database, which guarantees a considerably stronger statistical reliability and robustness than the AAMI standard. We choose SVM method during the evaluation because accroding to section III.B, SVM outperforms the multiple linear regression and decision tree methods, by showing lower MAE and STD at the same time, in both SBP and DBP estimation.

2) EVALUATION WITH BRITISH HYPERTENSION SOCIETY (BHS) STANDARD

Table 4 presents an evaluation of the proposed methodology using the SCSA features alone and SVM learning by the BHS standard. BHS grades BP measurement devices based on their cumulative percentage of errors under three different thresholds, i.e., 5, 10, and 15 mmHg [13]. According to the BHS standard, the proposed method is consistent with the grade B in the estimation of DBP and with the grade B in the estimation of the MAP value. MAP is very close to grade A in terms of the 15 percent cumulative error percentage. We achieved 92.77% compared to 95%, while meeting the rest of the standard for more than 6.41% in the 10 percent cumulative error percentage and 9.18% in the 5 percent cumulative error percentage. This suggests that we comprehend most of the cases estimation accurately with the SCSA features and while leaving around 10% of testing samples out of the 15 mmHg range, our method performs well in the rest of the cases.

3) COMPARISON WITH OTHER WORKS

To perform a fair comparison, all algorithms summarized in Table 5 are executed in the same database in terms of the number of individuals and types of database. Features used in this comparison are summarized in subsection II-C2. Most cuffless ABP estimation methods utilize PPG or ECG signal waveforms when analysing ABP values [2], [3], [7]–[9], [11], [23], [31]. In comparison, our method extracts more information from PPG by presenting better results than [3], [32] and [8]. PPG features are used in [3], where waveform width and area are used as features. [32] and [8] use PAT features only, showing results which are comparable with [3] which uses PPG signal only. One can see from Table 5 that our method performs better by showing better accuracy in DBP and MAP. This results from the components localization (shown in Fig. 4 and 5) of the systolic and diastolic peaks of the PPG signal. Since both PPG and ECG contains important information of arterial blood pressure, [9] further combines ECG and PPG signals by proposing a good summary of ECG and PPG feature set while achieving reasonable accuracy. It is worthwhile to mention that [9] presents comprehensive summary of existing methods and in comparison, our work presents comparable results in terms of DBP and MAP by using a combination PPG and ECG feature set.

III. NEURAL NETWORK BASED BP ESTIMATION

There are various ANN architectures for fitting the input data to target, such as counter propagation, learning vector quantization, and radial basis function. Despite good performance, these architectures require large numbers of neurons and cannot be applied in the case of a big training set, due to their substantial memory requirements.

In this paper, PPG features are fed to a multilayer feed forward neural network (FFNN) architecture, which has 14 input neurons (the number of input parameters, as mentioned above) and 3 output neurons, to simultaneously estimate SBP, DBP and MAP. This architecture is shown in Fig. 12.

The loss function of the neural network is defined as follows:

$$L(t) = \frac{1}{2m}\sum_{i=1}^{m}(y_i - \hat{y}_i) \tag{14}$$

where m is the number of samples, $\hat{y}$ and y are expected output and reference output respectively. Cosidering this NN structure is for small and middle scale problems such as BP regression, Levenberg-Marquardt (LM) algorithms are utilized in the network back-propagation training process. The approximated Hessian H is given by

$$H = J^T J + \mu I, \tag{15}$$

where $\mu > 0$ and J denotes the Jacobian matrix of loss function eq. 14. The Levenberg-Marquardt algorithm uses this approximated Hessian matrix iterative update hidden layer weights W in a newton like way:

$$W_{k+1} = W_k - [J^T J + \mu I]^{-1} J^T e, \tag{16}$$

Fig. 13 shows the histograms of the errors, calculated as the difference between real SBP & DBP and the output of the

TABLE 5. Comparison with other works.

Literature works	DBP		MAP		SBP	
	STD (mmHg)	MAE (mmHg)	STD (mmHg)	MAE (mmHg)	STD (mmHg)	MAE (mmHg)
This work (SCSA features only)	5.649	5.087	5.158	5.157	7.309	7.395
This work (PAT-included features)	5.537	4.881	4.947	4.857	6.954	6.887
Cuffless-ECG [9]	5.721	4.530	4.721	4.243	6.675	5.752
PTT [34]	6.439	6.399	6.002	6.185	8.619	9.049
PTT-inverse [8]	7.141	19.246	-	-	10.249	10.838
PPG-only [3]	7.408	5.875	5.706	5.337	7.672	6.997

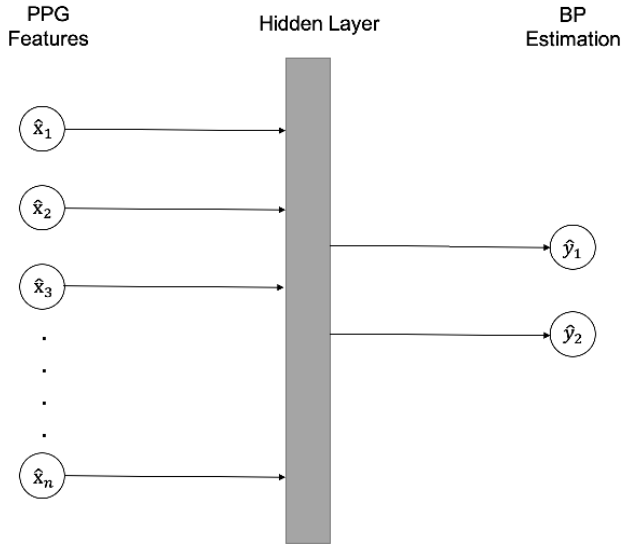

FIGURE 12. The block diagram of neural network estimation methodology. Input laye: SCSA extracted features used by separate input nodes. Hidden layer: Node numbers tuned to increase network performance (typically 10). Output layer: SBP and DBP collected for each corresponding input sample.

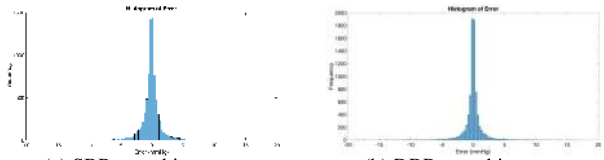

(a) SBP error histogram (b) DBP error histogram

FIGURE 13. SBP and DBP error histogram from the FFNN estimation.

FFNN, for the proposed method. The mean difference and standard deviation between the estimated BP and measured BP are -0.0252 ± 4.8569 mmHg for DBP and 0.0349 ± 6.4477 mmHg for SBP, which meets the ISO standars. [14].

IV. DISCUSSION

A. SUPERVISED MACHINE LEARNING TECHNIQUES

Compared to other literature works, our advantage lies in the fact that only one PPG sensor is required. The sensor can be easily placed at the finger level, which pushes the limit of easy implementation of cuff-less BP estimation. Our methods presents promising results, in terms of MAE and STD, comparable with [2], which comprehensively combines

TABLE 6. Results evaluated by the AAMI standard (FFNN).

		ME (mmHg)	STD (mmHg)	subjects
Our results	MAP	-	-	-
	DBP	-0.0252	4.8569	7993
	SBP	-0.0349	6.4477	7993
AAMI [14]		≤ 5	≤ 8	≥ 85

TABLE 7. Comparison with the BHS standard (FFNN).

		Cumulative Error Percentage		
		≤ 5 mmHg	≤ 10 mmHg	≤ 15 mmHg
Our results	SBP	96.62%	99.22%	99.74%
	DBP	97.36%	99.41%	99.85%
	MAP	-	-	-
BHS [13]	grade A	60%	80%	95%
	grade B	50%	75%	90%
	grade C	40%	65%	85%

PPG features and ECG PAT features shown in [3], [8], [32]. While combining PPG and ECG features presents the best performance, the significance of our work lies in the fact that only PPG signals are used, which is far more convenient comparing to using ECG and PPG simultaneously. The study developed and compared three machine learning algorithms to estimate ABPs using SCSA extracted features from PPG signal and revealed that the support vector machine (SVM) algorithm was the best approach with overall acceptable estimation accuracy. According to the BHS [13], our proposed method (PPG features only) has grade B in estimation of the DBP and MAP, with performance close to the grade A margin. Without the need of continuous ECG measurement (also avoiding synchronization issues), our method provides more potential in mobile healthcare equipments to monitor the ABP continuously, while not causing inconvenience or discomfort for individuals.

B. NEURAL NETWORK ESTIMATION

Studies such as [2] has the problem of SBP not meeting AAMI standard [14]. While some other studies have claimed to have met this condition, after applying their features and implementing on MIMIC II database, the accuracy slightly decreases. We believe that this is an universal issue in the BP regression framework. As a result, a new algorithm scheme is needed for this accuracy issue.

To solve the problem of large STD values of SBP estimation, a FFNN structure is proposed to increase the SBP estimation accuracy. Similarly in the previous section, we use AAMI and BHS standard to evaluate this algorithm. We found that the proposed ABP estimation algorithm works properly, with estimation accuracy meeting ISO standard [14]. According to the BHS standard [13], our proposed method (PPG features only) has grade A in estimation of the DBP and SBP, with performance far exceeding the grade A margin.

This study has limitations. First, it should be pointed out that the MIMIC II database is based on patients from intensive care units (ICU), whose ABPs are inevitably affected by drugs. Also, the age of patients are higher than average due to usage of ICU records, thus putting more challenge on the ABP estimation algorithms. Further, PPG signal segments are preprocessed when extracting features, while previous work [27] has shown SCSA method to be robust against noise, it is worthwhile to implement the algorithms in a non-preprocessed database and analyse the robustness of feature extraction. Finally, this study will be further extended to other clinical database with different BP categories (normotensive, hypertensive, and hypotensive) to further analyse BP classification by using PPG signal.

V. CONCLUSION

In this paper, we have solved the problem of continuous ABP estimation by utilizing a single noninvasive PPG sensor. A noninvasive, cuff less, calibration-free, and continuous BP estimation approach is proposed based on the semi classical signal analysis (SCSA). This is the first study that presents a completely new way of PPG signal feature extraction using SCSA. The proposed methods are tested through MIMC II database which contains a large volume of samples, demonstrating robustness and statistical reliability. Primarily, the proposed methodology consists of signal preprocessing, feature extraction, and regression stages. It is shown that the proposed ABP estimation algorithm works properly, with estimation accuracy meeting ISO standard [14]. The importance of this study is that, aside from testing existing methods on MIMIC II database over a large range of samples, SCSA can extract features even when the localization of inflection point on PPG signal is difficult or simply impossible due to drugs or abnormal physical situation, guaranteeing stable performance of BP estimation in such situations.

In addition to BP estimation methods based on supervised machine learning we propose a high SBP estimation scheme to obtain the level of accuracy in [14]. This is achieved using a typical-structure feed forward neural network. According to the Association for the Advancement of Medical Instrumentation (AAMI), the mean and deviation absolute error between the device estimation and the reference SBP values is less than 5 ± 8 mmHg, and we are one of the few studies to achieve such accuracy. With the wearable PPG sensor becoming an increasingly popular technology, this method has practical significance as part of a big data solution.

As a future work, in order to improve the comprehensiveness of this work, the following ideas could be tested:

1) To further estimate effectiveness of the proposed methods, data from healthy people are recommended to be used for data training, in addition to patients' data from MIMIC II database.
2) It could be interesting to consider different clinical BP categories (normotensive, hypertensive, and hypotensive). The proposed methods would for instance aid to distinguish patients' BP categories by PPG signals only, which might be of clinical significance.

VI. CODE AND DATA AVAILABILITY

The MIMIC II database used in this study is access available in the link (https://archive.ics.uci.edu/ml/datasets/Cuff-Less+Blood+Pressure+Estimation).

The code used in this study is available upon request to the authors in this paper.

REFERENCES

[1] C. Höcht, "Blood pressure variability: Prognostic value and therapeutic implications," *Hypertension*, vol. 2013, Jun. 2013, Art. no. 398485.
[2] X.-R. Ding, Y.-T. Zhang, J. Liu, W.-X. Dai, and H. K. Tsang, "Continuous cuffless blood pressure estimation using pulse transit time and photoplethysmogram intensity ratio," *IEEE Trans. Biomed. Eng.*, vol. 63, no. 5, pp. 964–972, May 2016.
[3] S. G. Khalid, J. Zhang, F. Chen, and D. Zheng, "Blood pressure estimation using photoplethysmography only: Comparison between different machine learning approaches," *J. Healthcare Eng.*, vol. 2018, pp. 1–13, Oct. 2018.
[4] G. Parati, J. E. Ochoa, C. Lombardi, and G. Bilo, "Assessment and management of blood-pressure variability," *Nature Rev. Cardiol.*, vol. 10, no. 314, pp. 55–143, 2014.
[5] J. R. Higgins and M. de Swiet, "Blood-pressure measurement and classification in pregnancy," *Lancet*, vol. 357, no. 9250, pp. 131–135, Jan. 2001. [Online]. Available: http://www.sciencedirect.com/science/article/pii/S0140673600035522
[6] A. De and L. Sierra, "Ambulatory blood pressure monitoring is a useful tool for all patients," *Hipertens Riesgo Vascular*, vol. 34, pp. 45–49, Jul. 2017.
[7] H. Gesche, D. Grosskurth, G. Küchler, and A. Patzak, "Continuous blood pressure measurement by using the pulse transit time: Comparison to a cuff-based method," *Eur. J. Appl. Physiol.*, vol. 112, no. 1, pp. 309–315, Jan. 2012.
[8] M. Masè, W. Mattei, R. Cucino, L. Faes, and G. Nollo, "Feasibility of cuff-free measurement of systolic and diastolic arterial blood pressure," *J. Electrocardiology*, vol. 44, no. 2, pp. 201–207, Mar. 2011.
[9] M. Kachuee, M. M. Kiani, H. Mohammadzade, and M. Shabany, "Cuffless blood pressure estimation algorithms for continuous health-care monitoring," *IEEE Trans. Biomed. Eng.*, vol. 64, no. 4, pp. 859–869, Apr. 2017.
[10] P. M. Nabeel, J. Joseph, and M. Sivaprakasam, "Magnetic plethysmograph transducers for local blood pulse wave velocity measurement," in *Proc. 36th Annu. Int. Conf. IEEE Eng. Med. Biol. Soc.*, Aug. 2014, pp. 1953–1956.
[11] J. Allen, "Photoplethysmography and its application in clinical physiological measurement," *Physiolog. Meas.*, vol. 28, no. 3, pp. R1–R39, Feb. 2007, doi: 10.1088%2F0967-3334%2F28%2F3%2Fr01.
[12] S. S. Mousavi, M. Firouzmand, M. Charmi, M. Hemmati, M. Moghadam, and Y. Ghorbani, "Blood pressure estimation from appropriate and inappropriate PPG signals using a whole-based method," *Biomed. Signal Process. Control*, vol. 47, pp. 196–206, Jan. 2019. [Online]. Available: http://www.sciencedirect.com/science/article/pii/S1746809418302209
[13] P. M. Nabeel, J. Joseph, and M. Sivaprakasam, "Magnetic plethysmograph transducers for local blood pulse wave velocity measurement," *J. Hypertension*, vol. 11, no. 2, pp. 43–62, 1993.
[14] *American National Standard for Electronic or Automated Sphygmomanometers*, document PANSI/AAMI SP 10 2002, Association for the Advancement Instrumentation, Arlington, VA, USA, 2002.

[15] T.-M. Laleg-Kirati, E. Crépeau, and M. Sorine, "Semi-classical signal analysis," *Math. Control, Signals, Syst.*, vol. 25, no. 1, pp. 37–61, Mar. 2013.
[16] T.-M. Laleg-Kirati, C. Médigue, Y. Papelier, F. Cottin, and A. Van de Louw, "Validation of a semi-classical signal analysis method for stroke volume variation assessment: A comparison with the PiCCO technique," *Ann. Biomed. Eng.*, vol. 38, no. 12, pp. 3618–3629, Dec. 2010, doi: 10.1007/s10439-010-0118-z.
[17] C. S. Gardner, J. M. Greene, M. D. Kruskal, and R. M. Miura, "Korteweg-devries equation and generalizations. VI. methods for exact solution," *Commun. Pure Appl. Math.*, vol. 27, no. 1, pp. 97–133, Jan. 1974. [Online]. Available: https://onlinelibrary.wiley.com/doi/abs/10.1002/cpa.3160270108
[18] T.-M. Laleg, E. Crepeau, Y. Papelier, and M. Sorine, "Arterial blood pressure analysis based on scattering transform i," in *Proc. 29th Annu. Int. Conf. IEEE Eng. Med. Biol. Soc.*, Aug. 2007, pp. 5326–5329.
[19] T.-M. Laleg, C. Medigue, F. Cottin, and M. Sorine, "Arterial blood pressure analysis based on scattering transform II," in *Proc. 29th Annu. Int. Conf. IEEE Eng. Med. Biol. Soc.*, Aug. 2007, pp. 5330–5333.
[20] E. Crépeau and M. Sorine, "A reduced model of pulsatile flow in an arterial compartment," *Chaos, Solitons Fractals*, vol. 34, no. 2, pp. 594–605, Oct. 2007. [Online]. Available: http://www.sciencedirect.com/science/article/pii/S0960077906002888
[21] T.-M. Laleg, E. Crépeau, and M. Sorine, "Separation of arterial pressure into a nonlinear superposition of solitary waves and a windkessel flow," *Biomed. Signal Process. Control*, vol. 2, no. 3, pp. 163–170, Jul. 2007.
[22] G. Martínez, N. Howard, D. Abbott, K. Lim, R. Ward, and M. Elgendi, "Can photoplethysmography replace arterial blood pressure in the assessment of blood pressure?" *J. Clin. Med.*, vol. 7, no. 10, p. 316, Sep. 2018.
[23] J. D. Buxi and M. Yuce, "Cuffless blood pressure estimation from the carotid pulse arrival time using continuous wave radar," in *Proc. 37th Annu. Int. Conf. IEEE Eng. Med. Biol. Soc. (EMBC)*, Aug. 2015, pp. 5704–5707.
[24] J. Yi Kim, B. Hwan Cho, S. Mi Im, M. Ju Jeon, I. Young Kim, and S. I. Kim, "Comparative study on artificial neural network with multiple regressions for continuous estimation of blood pressure," in *Proc. IEEE Eng. Med. Biol. 27th Annu. Conf.*, Jan. 2005, pp. 6942–6945.
[25] M. Kachuee, M. M. Kiani, H. Mohammadzade, and M. Shabany, "Cuffless high-accuracy calibration-free blood pressure estimation using pulse transit time," in *Proc. IEEE Int. Symp. Circuits Syst. (ISCAS)*, May 2015, pp. 1006–1009.
[26] A. Chahid, S. Bhaduri, M. Maoui, E. Achten, H. Serrai, and T. Laleg-Kirati, "Residual water suppression using the squared eigenfunctions of the Schrödinger operator," *IEEE Access*, vol. 7, pp. 69126–69137, 2019, doi: 10.1109/ACCESS.2019.2918286.
[27] P. Li and T. M. Laleg-Kirati, "Signal denoising based on the Schrödinger operator's eigenspectrum and a curvature constraint," 2019, *arXiv:1908.07758*. [Online]. Available: https://arxiv.org/abs/1908.07758
[28] L. Wang and Y. T. Zhang, "A novel photoplethysmogram index for total peripheral resistance after bicycle exercise," in *Proc. 5th Int. Conf. Ubiquitous Healthcare*, 2008.
[29] L. Wang, E. Pickwell-MacPherson, Y. P. Liang, and Y. T. Zhang, "Noninvasive cardiac output estimation using a novel photoplethysmogram index," in *Proc. Annu. Int. Conf. IEEE Eng. Med. Biol. Soc.*, Sep. 2009, pp. 1746–1749.
[30] K. Takazawa, N. Tanaka, M. Fujita, O. Matsuoka, T. Saiki, M. Aikawa, S. Tamura, and C. Ibukiyama, "Assessment of vasoactive agents and vascular aging by the second derivative of photoplethysmogram waveform," *Hypertension*, vol. 32, no. 2, pp. 365–370, Aug. 1998.
[31] V. Chandrasekaran, R. Dantu, S. Jonnada, S. Thiyagaraja, and K. P. Subbu, "Cuffless differential blood pressure estimation using smart phones," *IEEE Trans. Biomed. Eng.*, vol. 60, no. 4, pp. 1080–1089, Apr. 2013.
[32] C. Douniama, C. Sauter, and R. Couronne, "Blood pressure tracking capabilities of pulse transit times in different arterial segments: A clinical evaluation," in *Proc. 36th Annu. Comput. Cardiol. Conf. (CinC)*, Sep. 2009, pp. 201–204.

PEIHAO LI received the B.S. degree in observation, navigation, and control from Northwestern Polytechnical University, China. He is currently pursuing the Ph.D. degree with the Department of Electrical Engineering, Division of Computer, Electrical and Mathematical Sciences and Engineering (CEMSE), King Abdullah University of Science and Technology (KAUST). He joined the M.S./Ph.D. Program in electrical engineering with KAUST in Fall 2016. He is especially interested in signal processing based on the Schrödinger Operator and SCSA method. His research interests include signal processing and applications in biomedical and signal processing field.

TAOUS-MERIEM LALEG-KIRATI (Senior Member, IEEE) received the master's degree in control systems and signal processing from University of Paris 11, France, and the Ph.D. degree in applied mathematics from Inria, Paris, in 2008. From 2009 to 2010, she was working as a Permanent Research Scientist with the French Institute for research in Computer Sciences and Control Systems (INRIA), Bordeaux. She joined King Abdullah University of Science and Technology (KAUST), in December 2010, where she is currently an Associate Professor with the Division of Computer, Electrical and Mathematical Sciences and Engineering, KAUST. She considers applications in engineering and biomedical fields. Her research interests include modeling, estimation, and control of complex systems and signal/image analysis.